Oxygen-vacancy-rich Ru-clusters decorated Co/Ce oxides modifying ZIF-67 nanocubes as a high-efficient catalyst for $NaBH_4$ hydrolysis

Luyan Shi [a], *Ke Zhu* [a], *Yuting Yang* [a], *Yi Liu* [a], *Shoulei Xu* [c,***], *Tayirjan Taylor Isimjan* [b,**], *Xiulin Yang* [a,*]

[a] *G ang i Ke Labo a o of Le Ca bon Ene g Ma e ial , School of Chemi and Pha mace ical Science , G ang i No mal Uni e i , G ilin 541004, China*

[b] *Sa di A abia Ba ic Ind ie Co po a ion (SABIC) a King Abd llah Uni e i of Science and Technolog (KAUST), Th e al 23955-6900, Sa di A abia*

[c] *School of Ph ical Science and Technolog , G ang i Uni e i , 100 Ea Da e Road, Nanning 530004, China*

HIGHLIGHTS

- Ru/Co_6Ce_1@ZIF-67 nanocubes are fabricated b surfactant-mediated and reduction methods.
- The catal st sho s a high HGR and TOF (413.9 min^{-1}) surpassing most recentl reported catal sts.
- The catal st e hibits a stable multi-c cle reusabilit for $NaBH_4$ h drol sis.
- O gen vacancies and the s nerg bet een different components are the ke s to improve catal tic activit .

GRAPHICAL ABSTRACT

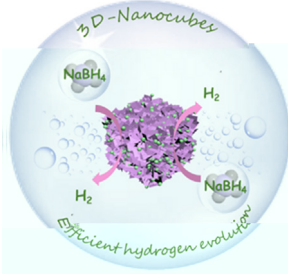

ARTICLE INFO

A icle hi o :
Received 13 Jul 2022
Received in revised form
26 August 2022
Accepted 29 August 2022
Available online 17 September 2022

Ke e o d :
Ru/Co_6Ce_1@ZIF-67 catal st
O gen vacancies

ABSTRACT

Designing a cost-effective and high-performance catal st for $NaBH_4$ h drol sis is a sig- ni cant step in developing a sustainable h drogen source. Herein, e prepared a cost-effective Ru-clusters decorated cobalt-cerium o ides coating ZIF-67 (Ru/Co_6Ce_1@ZIF-67) catal st via a facile reduction method, displa ing high performance and e ceptional reusabilit in alkaline $NaBH_4$ solution. The optimi ed catal st e hibits a high h drogen generation rate (HGR, 5726.1 mL min^{-1} g^{-1}), turnover frequenc (TOF, 413.9 mol_{H2} min^{-1} mol_R^{-1}), and lo activation energ (E_a, 53.0 kJ mol^{-1}), surpassing most of the recentl re- ported catal sts. Furthermore, the catal tic performance does not change considerabl after ve c cles, indicating the catal st's multi-c cle reusabilit . Studies impl the uniquel

* *Co e ponding a ho .*
** *Co e ponding a ho .*
*** *Co e ponding a ho .*
E-mail addresses: sl@g u.edu.cn (S. Xu), isimjant@sabic.com (T.T. Isimjan), l ang@g nu.edu.cn (X. Yang).

$NaBH_4$ h drol sis
H drogen generation

s nergistic effect of Ru, Co/Ce o ides, abundant o gen vacancies, as ell as the porous nanocube structure, enabling the catal sts to possess high metal dispersion, outstanding catal tic performance and e ceptional reusabilit . This ork ill open light on using an o gen vacancies-rich strateg to design a high-activit catal st for promoting $NaBH_4$ h drol sis.

Introduction

Energ shortage and environmental pollution are the main factors affecting the qualit of life [1]. There is a desperate need to mine green, rene able and ef cient energ materials [2,3]. H drogen is an ideal alternative to traditional fuels due to its high energ densit and ero CO_2 emission [4,5]. Ho ever, nding a cheap h drogen storage method is often ver challenging. $NaBH_4$ is a promising candidate among the various storage materials because of its high theoretical h drogen content of 10.6 t%, long-term stabilit in alkaline condition and nonto icit [6,7]. $NaBH_4$ can also generate H_2 through h - drol sis under mild conditions, and the b -products are non-to ic [8]. Moreover, a recent stud indicated that the $NaBH_4$ could be regenerated through b -product reh drogenation, making it possible for the $NaBH_4$–H_2-PEMFC s stem to be a primar source for on-demand po er suppl [9]. Nevertheless, the self-h drol sis of $NaBH_4$ releases H_2 slo l , and the overall conversion is onl 7–8% at ambient temperature [10,11]. Consequentl , designing ef cient catal sts to promote sodium boroh dride h drol sis remains a critical issue.

Previous studies suggested that noble metal-based cata-l sts, such as Ru–Co-PEDOT [12] and Ru–Fe/Go [13], sho ed e cellent catal tic activit and robust stabilit to ard $NaBH_4$ h drol sis [14]. Ho ever, the high cost, the lack of reserves, and the self-agglomeration limit industrial application [15,16]. Therefore, considerable afford has been dedicated to devel-oping non-noble transition metals. Recentl , cobalt-based catal sts are idel studied for h drol sis of sodium boro-h dride due to the fact that its performance is particularl validated as the most effective non-noble metal among Ni-, Fe-, and Cu-based catal sts [17]. Among cobalt-based cata-l sts, cobalt o ides have been con rmed to be ef cient cata-l st [18]. Wei et al. [19] reported that Co_3O_4 hollo ber catal st e hibited good performance. Ho ever, the activit and stabilit of cobalt o ides catal sts ere still lo er than those of noble metal catal sts [20]. Man noble metal and cobalt o ide composite catal sts have been developed to achieve high performance hile reducing costs. For e ample, Dou et al. [21] reported a high-ef cienc Ru-clusters decorated CoO @NPC catal st for h drogen generation.

To address the aggregation of the metal nanoparticles during s nthesis, suitable supports or organic capping agents should be introduced. Metal-organic frame orks (MOFs) are considered ideal support materials due to their unique prop-erties, including e ceptional porosit , structural diversit , large speci c surface area, and chemical stabilit [22,23]. ZIF-67 is one of MOFs ith imida ole as an organic linker ith metal cobalt, hich has a large speci c surface area to prevent metal particles agglomeration and has proven to be highl stable in solution, even in alkaline solution at high tempera-tures [24,25]. Man studies have also sho n that ZIF-67-supported composites catal sts e hibit remarkable perfor-mance in $NaBH_4$ h drol sis for h drogen production, e.g., Pd/PD-ZIF-67 [15], Ru/ZIF-67 [26] and so on. Given these merits, ZIF-67 appears to be an e cellent substrate to promote $NaBH_4$ h drol sis. Nonetheless, MOFs as carriers have lo electrical conductivit , hindering the charge transfer during h drol sis [27]. It can enhance electron transport b introducing o gen vacancies created b rare earth elements, such as cerium o ide [28]. In cerium o ides, Ce^{3+} and Ce^{4+} coe ist, and the electronic structure of Co species can be modi ed due to the e istence of electronicall e ible transitions and abundant o gen vacancies bet een Ce^{3+} and Ce^{4+}, thereb enhancing the conductivit of Co-MOF and improving the performance of the catal st [29,30]. Based on the above consideration, e as-sume that Ru cluster-modi ed Co o ides and doped Ce o ides have the potential to be an ef cient catal st for h drol sis of sodium boroh dride.

Here, e propose a facile surfactant-mediated and chemi-cal reduction method to s nthesi e Ru/Co_6Ce_1@ZIF-67 catal st ith abundant o gen vacancies for $NaBH_4$ h drol sis in alkaline environments. The Ru clusters (2.7 nm) decorated Co_6Ce_1@ZIF-67 nanocubes sho ed outstanding catal tic activit and remarkable reusabilit for $NaBH_4$ h drol sis. It has a high HGR value of 5726.1 mL min^{-1} g^{-1} and a TOF value of 413.9 mol_{H2} min^{-1} mol_R^{-1}. S stematic investigations further demonstrate that the ZIF-67 support prevents Ru clusters ag-gregation, and o gen vacancies can accelerate electronic transfer, promoting the reversible dissociation of B–H on active sites of Co o ides and Ru clusters, and nall stimulating h drol sis of sodium boroh dride. Furthermore, e proposed a plausible reaction mechanism according to the Michaelis-Menten model reported in the previous literature [31].

Experimental section

Materials

Cobalt nitrate he ah drate ($Co(NO_3)_2 \cdot 6H_2O$, 99.0%, Aladdin), cerium nitrate he ah drate ($Ce(NO_3)_3 \cdot 6H_2O$, 99.95%, Macklin), ruthenium (III) trichloride ($RuCl_3 \cdot H_2O$, 99%, Ru:37–40%, Innochem), 2-meth limida ole (2-MI, 98%, Aladdin), cet l-trimeth lammonium bromide (CTAB, 99.0%, Aladdin), sodium boroh dride ($NaBH_4 \geq 98.0\%$, Sinopharm Group), sodium h - dro ide (NaOH ≥

companies and could be used directl ithout further puri cation.

Synthesis of ZIF-67 nanocubes

Co-based eolitic imida olate frame ork (ZIF-67) nanocubes ere prepared according to previous ork ith slightl modi cation [32]. In a t pical procedure, 580 mg of $Co(NO_3)_2 \cdot 6H_2O$ as dissolved in 20 mL of deioni ed ater containing 10 mg of CTAB. Then, this solution as rapidl injected into 140 mL of an aqueous solution containing 908 mg of 2-meth limida ole and stirred at room temperature for 20 min. The purple product as collected b centrifugation, ashed three times ith ethanol and vacuum-dried at 70 °C for 12 h.

Synthesis of Co_6Ce_1@ZIF-67

A total of 60 mg of ZIF-67 nanocubes as dispersed in 40 mL of ethanol to form solution A. 160 mg of $Co(NO_3)_2 \cdot 6H_2O$ and 40 mg of $Ce(NO_3)_3 \cdot 6H_2O$ ere dissolved in 10 mL of ethanol to form solution B. Then, solution B as dripped on solution A under magnetic stirring and sonicated for 40 min to form a uniform solution. Finall , the product as collected b centrifugation, ashed ith ethanol three times, and vacuum-dried at 70 °C for 12 h. For comparison, under keeping the total mass of the metal salt at 0.2 g, other CoCe@ZIF-67 composites ere prepared b altering the Co/Ce molar ration (1:1, 4:1, 6:1, 9:1, 12:1) during the s nthesis process. The Co@ZIF-67 and Ce@ZIF-67 ere prepared via the same routine ithout adding $Ce(NO_3)_3 \cdot 6H_2O$ or $Co(NO_3)_2 \cdot 6H_2O$.

Synthesis of Ru/Co_6Ce_1@ZIF-67

The Co_6Ce_1@ZIF-67 (80 mg) as added into a 50 mL glass beaker ith 20 mL of deioni ed ater and 15 mg of $RuCl_3 \cdot H_2O$. After continuous stirring for 4 h, 10 mL of 2.6 M $NaBH_4$ solution (including 2 t% NaOH) as added drop ise into the above mi ture. After stirring for another 0.5 h, the resultant product cr stal as separated b centrifugation, follo ed b multiple times ashing in deioni ed ater and ethanol, and subsequentl dried in a vacuum at 70 °C for 12 h. Inductive coupled plasma atomic emission spectroscop (ICP-AES) accuratel determined the content of Ru species (Table S1) and the sample ith 6.3 t% sho ed the highest catal tic performance. Samples ith Ru loadings of 4.5 t% to 10.6 t% ere prepared b the same method, using $RuCl_3 \cdot H_2O$ ith different mass. As a comparison, a mass ratio of 6.3 t% Ru as applied to s nthesi e all other contrastive catal sts. The Ru/Co@ZIF-67 and Ru/Ce@ZIF-67 ere prepared using the same procedure mentioned above ithout $Ce(NO_3)_3 \cdot 6H_2O$ or $Co(NO_3)_2 \cdot 6H_2O$. In addition, Ru@ZIF-67 as s nthesi ed b directl adding $RuCl_3 \cdot H_2O$ into ZIF-67 solution, follo ed b a similar reduction treatment.

Synthesis of single Ru

200 mg of $RuCl_3 \cdot H_2O$ as dissolved in 40 mL of deioni ed ater via ultrasonication. After continuous stirring for 30 min, 10 mL of $NaBH_4$ solution as added into the above mi ture. Finall , the black mi ture as centrifuged to collect the sediment, hich as ashed at least three times ith deioni ed ater and ethanol, then dried under vacuum.

Catalytic hydrolysis of $NaBH_4$ measurements

The evolved h drogen from the h drol sis of $NaBH_4$ as collected and measured ith a drainage method. A mi ed solution of 25 mL, containing 150 mL $NaBH_4$ and 0.4 t% NaOH, as injected to a three-necked round-bottom ask (100 mL), placed into a temperature-controlled ater bath oscillator to keep it at 25 °C during the h drol sis reaction. After 0.5 h, the prepared catal sts (10 mg) ere dispersed in the above solution, rapidl plugging the ask. The instantaneous ater volume changes ere monitored b an electronic balance connected to a computer. H drol sis of $NaBH_4$ as also carried out at different temperatures (298–318 K) to obtain the activation energ . For the reusabilit stud , the catal st as recollected, ashed ith deioni ed ater and ethanol, and dried in a vacuum at 70 °C after each c cle. The collected catal st from the previous test as transferred to each process's ne test solution. It as orth noting that the amount of motivation as the same as in the rst c cle e periment. All tests ere repeated three times to ensure reliable results.

Results and discussion

Synthetic method and crystallinity analysis

The design strateg of the Ru/Co_6Ce_1@ZIF-67 is illustrated in Fig. 1a. Firstl , ZIF-67 nanocubes are prepared through a surfactant-mediated method. After ard, the as-prepared ZIF-67 nanocubes ere mi ed ith $Co(NO_3)_2 \cdot 6H_2O$ and $Ce(NO_3)_3 \cdot 6H_2O$ to form Co–Ce o ides on the surface of ZIF-67 nanocubes. Finall , the Ru species are introduced into the Co_6Ce_1@ZIF-67 b an ambient temperature reduction for producing the Ru/Co_6Ce_1@ZIF-67. The cr stallinit of as-prepared catal sts is rst anal ed b X-ra diffraction (XRD). As sho n in Fig. 1b, pure ZIF-67 nanocubes and Ru/Co_6Ce_1@ZIF-67 share the same XRD patterns, hile the intensit of the peaks varies bet een them. Ho ever, there is no apparent diffraction peak of the cobalt-cerium o ides, impl ing the lo -loading and/or amorphous nature of the composite. Such amorphous characteristics are bene cial for catal tic materials ith higher performance than cr stalline material because the can suppl larger ion-accessible surface area and suf cient redo -active centers [33]. Furthermore, no characteristic peaks of Ru clusters are observed in the XRD pattern of Ru/Co_6Ce_1@ZIF-67 due to the lo Ru loading, hich the fu lattice fringes can con rm in the TEM images of Ru/Co_6Ce_1@ZIF-67 [34]. As sho n in Fig. 1c, e resort to the electron paramagnetic resonance

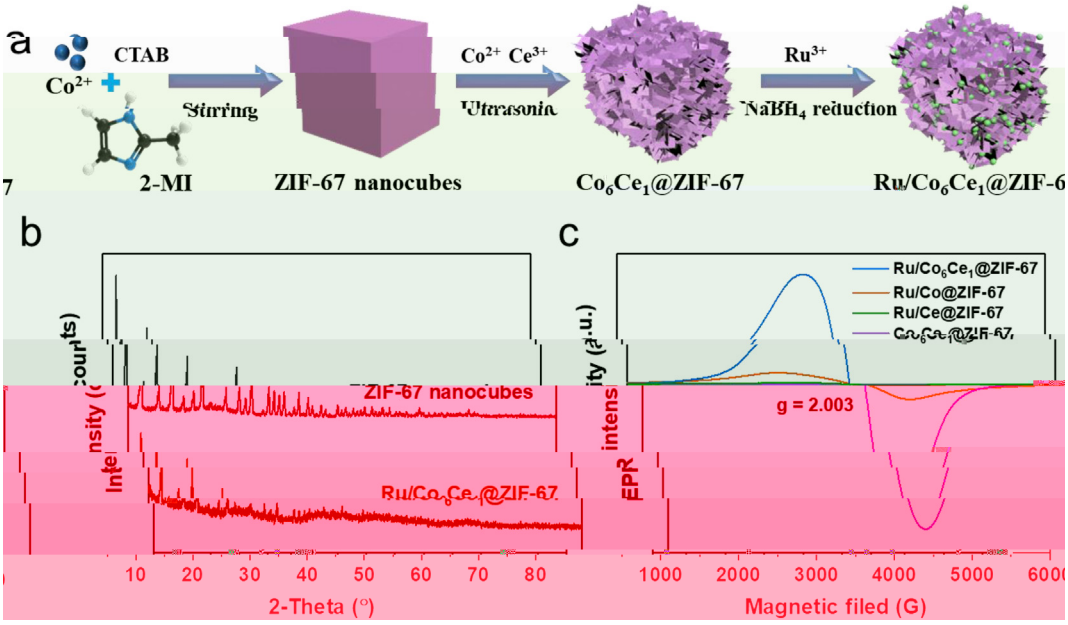

Fig. 1 – (a) Schematic diagram of the synthesis of Ru/Co_6Ce_1@ZIF-67. (b) XRD patterns of ZIF-67 nanocubes and Ru/Co_6Ce_1@ZIF-67. (c) EPR spectra of the synthesized Ru/Co_6Ce_1@ZIF-67, Ru/Co@ZIF-67, Ru/Ce@ZIF-67 and Co_6Ce_1@ZIF-67.

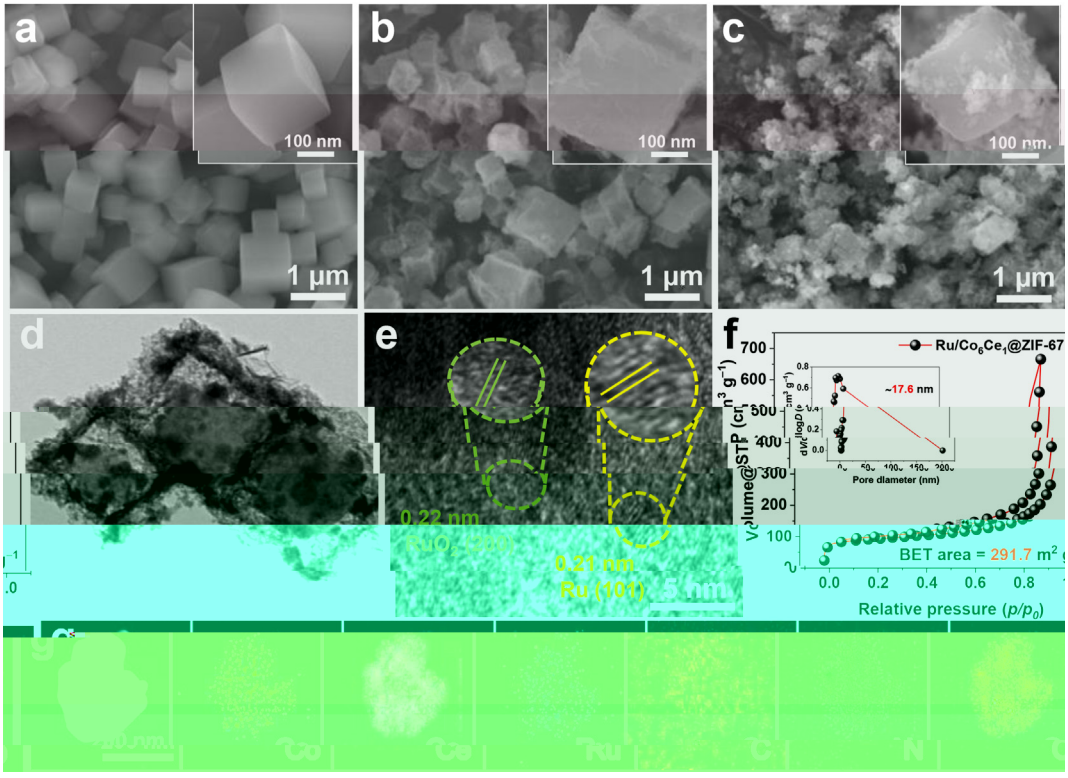

Fig. 2 – Scanning electron microscopy (SEM) of (a) ZIF-67 nanocubes, (b) Co_6Ce_1@ZIF-67 and (c) Ru/Co_6Ce_1@ZIF-67 (Insets are high-magnification SEM images). (d) Transmission electron microscopy (TEM) and (e) high-resolution TEM images of Ru/Co_6Ce_1@ZIF-67. (f) N_2 adsorption/desorption isotherms with pore-size distribution curve (inset) of Ru/Co_6Ce_1@ZIF-67. (g) HAADF-STEM image of Ru/Co_6Ce_1@ZIF-67 and corresponding elemental mappings of Co, Ce, Ru, C, N, and O.

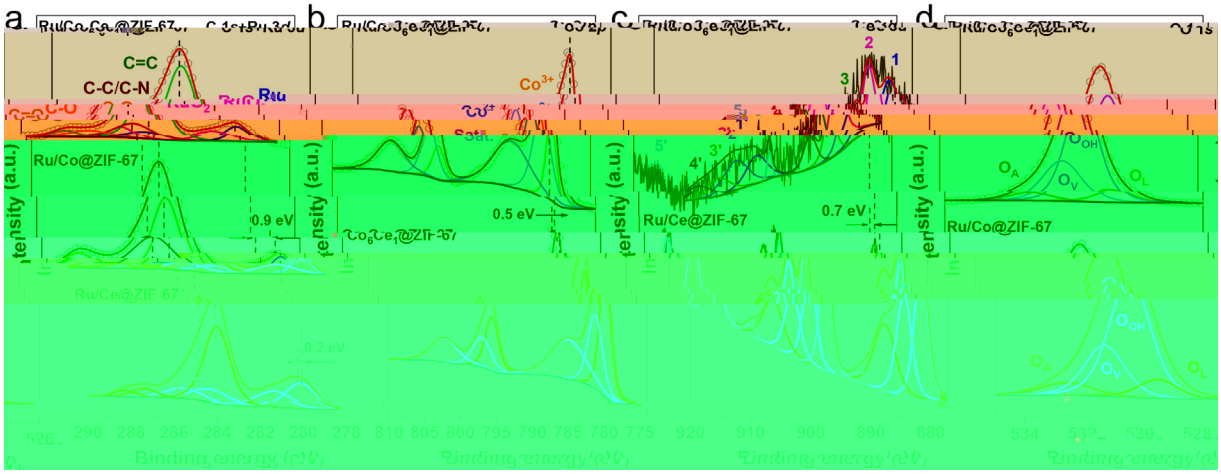

Fig. 3 – High-resolution XPS spectra of (a) C 1*s* + Ru 3*d*, (b) Co 2*p*, (c) Ce 3*d* and (d) O 1*s* regions of Ru/Co_6Ce_1@ZIF-67, Ru/Co@ZIF-67, Ru/Ce@ZIF-67 and Co_6Ce_1@ZIF-67, respectively.

Microstructure analysis

The morphological features and microstructure of the catal sts are anal ed b scanning electron microscop (SEM) and transmission electron microscop (TEM). Fig. 2a sho s the as-formed ZIF-67 nanocube morpholog ith a smooth surface. The further reaction ith e cess $Co(NO_3)_2{\cdot}6H_2O$ and $Ce(NO_3)_3{\cdot}6H_2O$ under sonication for 40 min leads to formation of Co_6Ce_1@ZIF-67 nanocubes. Fig. 2b reveals that the SEM image of Co_6Ce_1@ZIF-67 nanocubes still maintains the cubic shape. But the surface of the products become rough, and the higher magni cation image displa s that the Co_6Ce_1 o ides appear to be a nanosheet. After introducing Ru, the sample has cubic characteristics ith some distended nanoparticles on the surface, loosel stacked together (Fig. 2c). These results suggest that introducing a speci c number of Co/Ce o ides and Ru clusters does not destro the cube-like frame ork of the ZIF-67-based derivative. As sho in Fig. 2d, the TEM image sho s that Ru/Co_6Ce_1@ZIF-67 e hibits a olk-shell structure consisting of solid ZIF-67 olk and Ru/Co_6Ce_1 shell, similar to the literature reports [37,38]. Each nanocube is uniforml decorated ith dark Ru clusters ith a si e of 2.7 nm (Fig. S1). According to the high-resolution TEM image of Ru/Co_6Ce_1@-ZIF-67, Fig. 2e sho s that the lattice spacing of 0.21 nm are inde ed to Ru (101) cr stal plane [39]. The interplanar spacing of 0.22 nm are attributed to the (200) cr stal plane of RuO_2 [40]. The N_2 adsorption–desorption isotherms of Ru/Co_6Ce_1@ZIF-67 displa s the t pe IV isotherm ith a remarkable h steresis loop, indicating the e istence of mesopores [41]. The Brunauer-Emmett-Teller (BET) speci c surface area and pore si e are 291.7 $m^2\ g^{-1}$ and 17.6 nm (Fig. 2f). These results sho that the multiporous 3D frame structure and high surface area of Ru/Co_6Ce_1@ZIF-67 bene t ions' fast diffusion and e pose more active sites, hich can enhance the catal tic activit [42,43]. In addition, the EDX spectrum (Fig. S2) manifests the presence of Ru, Co, Ce, C, N, and O, and elemental mapping images elucidate that all the elements are homogenousl distributed throughout the Ru/Co_6Ce_1@ZIF-67 catal st (Fig. 2g).

X-ray photoelectron spectroscopy analysis

X-ra photoelectron spectroscop (XPS) has been further conducted to investigate the relationship bet een the charge and chemical valence states on the surface of the catal sts. As sho n in Fig. S3, the XPS surve spectra of Ru/Co_6Ce_1@ZIF-67 verif the presence of C, N, O, Co, Ce and Ru elements, agreeing ell ith the above HAADF-STEM elemental mapping and EDX results. The high-resolution C 1 + Ru 3*d* spectrum (Fig. 3a) are deconvoluted into C=C (284.0 eV), C–C (284.8 eV) and used as a calibration standard [44]. The t o peaks at 280.0 and 284.2 eV binding energies attribute to metallic Ru^0 [21], hereas the peaks at 281.2 eV and 285.4 eV correspond to RuO_2. This surface o ide could be formed from e posure of the samples to atmosphere during the reaction. Compared to the Ru/Co@ZIF-67, the binding energ of Ru is positivel shifted b 0.9 eV, indicating that the Ce doping can effectivel tune the electronic structure of Ru/Co_6Ce_1@ZIF-67, thereb regulating ef cient charge transfer [45]. Compared ith the Ru/Ce@ZIF-67 sample, the binding energ of Ru is negativel shifted b 0.2 eV, hich indicates that there is a strong charge-transfer interaction bet een Ru clusters and Co o ides [46]. Fig. 3b displa s the Co 2*p* high-resolution spectrum, here the binding energies of 779.5, 780.8 and 785.3 eV can be coincided ith Co^{3+}, Co^{2+}, and the satellite peak [47]. The binding energies of Co on Ru/Co_6Ce_1@ZIF-67 e hibit a negative shift compared to the Co_6Ce_1@ZIF-67, hich con- rms that the introduction of Ru clusters has a great in uence on the electronic states of the surrounding Co atoms. T pi-call , the Co^{2+}/Co^{3+} ratio of the Ru/Co_6Ce_1@ZIF-67 is higher than that of Co_6Ce_1@ZIF-67, suggesting that the part of Co^{3+} is reduced to Co^{2+} after introducing Ru to create o gen vacancies [48]. Interestingl , it has been reported that o gen vacancies can accelerate electronic transfer and increase the conductivit of the catal st, la ing the foundation for improving catal tic performance [49,50].

The Ce 3*d* spectrum of Ru/Co_6Ce_1@ZIF-67 is tted ith ve pairs of spin-energ separations (Fig. 3c). The characteristic peaks located at 880.9 eV, 887.3 eV (1, 3) and 899.5 eV, 905.9 eV

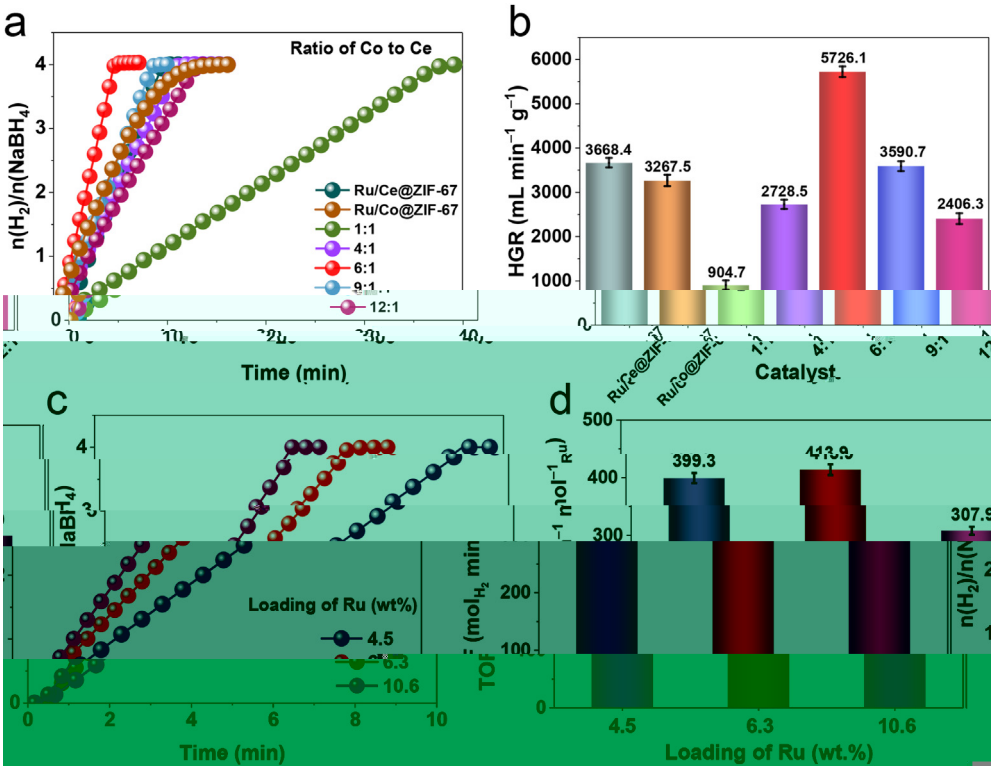

Fig. 4 – (a) Curves of hydrolysis of alkaline $NaBH_4$ solution with different rations of Co/Ce, and (b) the corresponding H_2 evolution rate values. (c) Curves of hydrolysis of alkaline $NaBH_4$ solution with different loadings of Ru species on Ru/Co_6Ce_1@ZIF-67 catalysts, and (d) the summarized TOF values.

(1′, 3′) are assigned to Ce^{3+} ($3d^{10}4f^1$ initial electronic state), hereas the si peaks at 884.4 eV, 890.6eV, 897.4eV (2, 4, 5) and 903.0 eV, 909.2 eV, 916.0 eV (2′, 4′, 5′) are attributed to Ce^{4+} ($3d^{10}4f^0$ initial electronic state) [51,52]. In the Ce 3*d* spectra, the Ce^{3+} co-e ists ith Ce^{4+} in the composite [53]. Clearl , the peak of Ce^{3+} in Ru/Co_6Ce_1@ZIF-67 sho s a negative shift of about 0.7 eV compared to Ru/Ce@ZIF-67, impl ing the electrostatic interactions bet een Ce o ides and surrounding Co o ides. It is orth noting that the Ce^{3+} ions interact ith surrounding atoms such as Co through lone electron e isting in the $4f^1$ orbital. In addition, o gen vacancies can be created on the catal st surface due to the charge compensation of Ce^{3+} ions [54]. The above anal ses prove that the introduction of Ce can generate more o gen vacancies, thereb enhancing the catal st's performance [55]. Furthermore, e detect the o gen vacancies b O 1 XPS spectra. Fig. 3d sho s that the O 1 spectra can be deconvoluted into four peaks. The peaks of 529.1 eV, 530.0 eV, 530.7 eV and 532.0 eV can be attributed to lattice o gen (O_L), o gen atoms bound to h dro l species (O_{OH}), o gen vacanc (O_v) and absorbed o gen (O_A), respectivel [56,57]. The integral area ratio of o gen vacanc peaks in Ru/Co_6Ce_1@ZIF-67 (26.3%) is more signi cant than that in Ru/Co@ZIF-67 (24.6%), impl ing that o gen vacancies increase after the introduction of Ce component, hich is in line ith the EPR results.

Catalytic hydrolysis analysis

The catal tic activities are assessed in alkaline $NaBH_4$ solution at 25 °C, and the volume of H_2 is measured b a ater displacement method. The h drol sis setup is schematicall illustrated in Fig. S4. The $NaBH_4$ (150 mM) aqueous solution sho s almost no self-h drol sis (Fig. S5), and negligible h drogen gas is produced from 150 mM $NaBH_4$ + 0.4 t% NaOH solution indicating $NaBH_4$ is stable in both ater and under an alkaline solution (Fig. S6). As sho n in Fig. 4a and b, e investigate the effect of catal sts fabricated b different molar ratios of Co/Ce on H_2 generation. When the molar ratio of Co/Ce is 6:1, Ru/Co_6Ce_1@ZIF-67 e hibits the best activit and is superior to those of Ru/Co@ZIF-67 and Ru/Ce@ZIF-67. And the HGR value is superior to those currentl reported literature (Table S2). Simultaneousl , the optimal Ru loading has been researched in great detail. As displa ed in Fig. 4c–d, a higher Ru loading sho s a higher H_2 release rate, but the TOF values sho a volcano-shape curve. When the content of Ru is 6.3 t %, the corresponding TOF reaches a ma imum value of 413.9 mol_{H2} min^{-1} mol_{Ru}^{-1}.

As sho n in Fig. 5a and b, the Ru/Co_6Ce_1@ZIF-67 catal st onl takes about 6 min to achieve the complete h drol sis of sodium boroh dride. Notabl , for Ru/ZIF-67 and Ru catal sts, sodium boroh dride h drol ed onl about 35% and 10% ithin 6 min, hile Co_6Ce_1@ZIF-67 and ZIF-67 had almost no activit . These results sho ed that Ru/Co_6Ce_1@ZIF-67 e hibited the highest performance relative to all control catal sts, indicating that Ru is the predominate active site and Co_6Ce_1@ZIF-67 pla s a crucial role in catal tic h drol sis [58]. The anal sis suggests that the s nergistic effect of different components and abundant o gen vacancies in the Ru/Co_6Ce_1@ZIF-67 h brid catal st are the main factors for the high catal tic performance. The in uence of $NaBH_4$ concentration

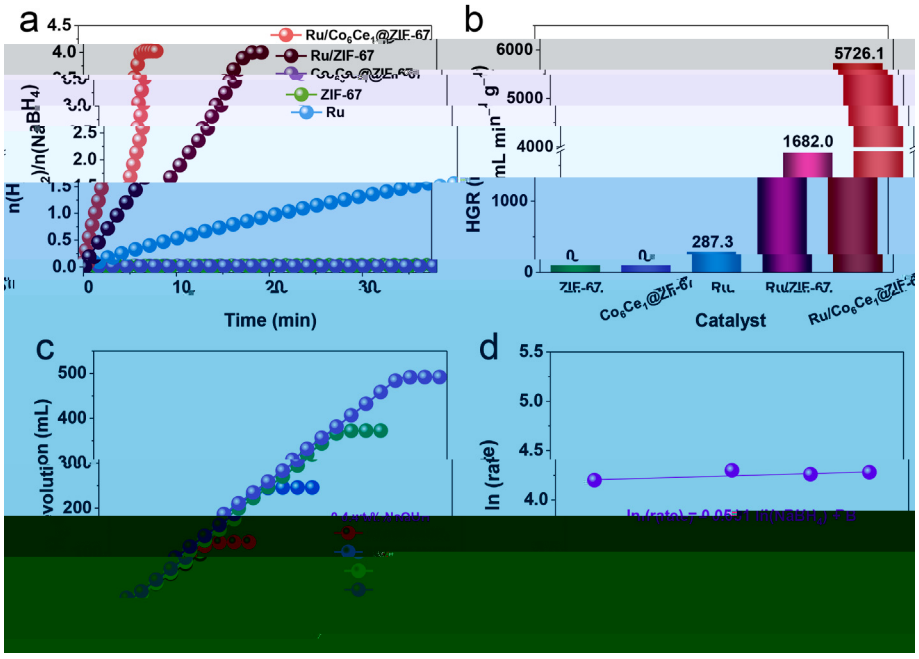

Fig. 5 – (a) Curves of hydrolysis of alkaline $NaBH_4$ solution with different kinds of catalysts, and (b) the corresponding H_2 evolution rate values. (c) The relationship between H_2 evolution and different $NaBH_4$ concentrations and (d) the corresponding plot of ln (rate) *vs* ln (concentration of $NaBH_4$).

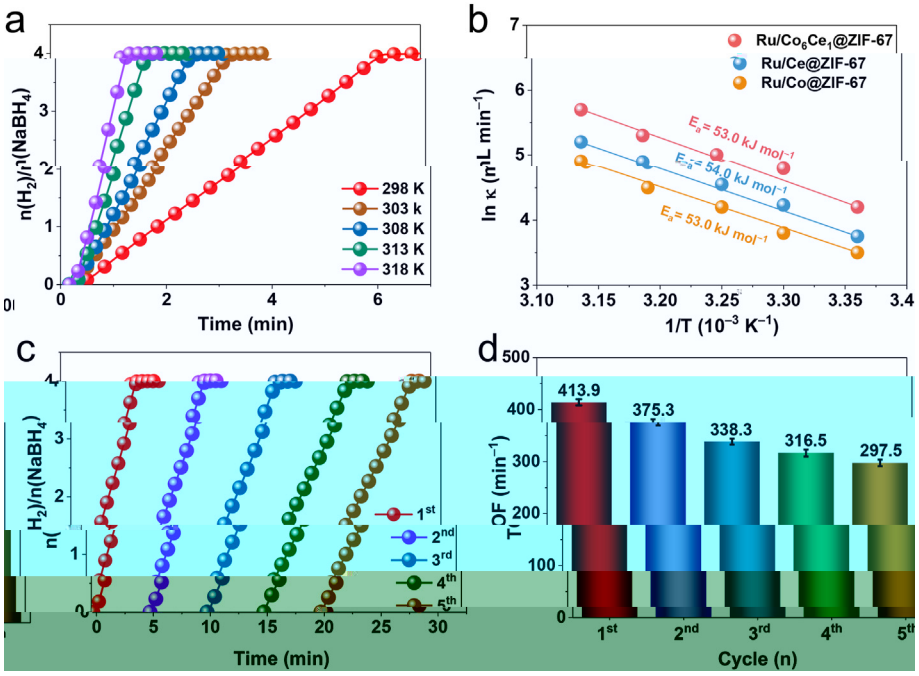

Fig. 6 – (a) Curves of hydrolysis of alkaline $NaBH_4$ solution with different reaction temperatures, and (b) the calculated activation energies of Ru/Co_6Ce_1@ZIF-67, Ru/Co@ZIF-67 and Ru/Ce@ZIF-67 catalysts. (c) Recycling stability test of Ru/Co_6Ce_1@ZIF-67 catalyst in alkaline $NaBH_4$ solution at 25 °C and (d) the corresponding TOF values in the different recycling test.

has also been e plored at 25 °C ith 10 mg Ru/Co_6Ce_1@ZIF-67. Fig. 5c reveals that the h drogen generation rate does not change signi cantl . Mean hile, the relation bet een ln (rate) and ln ($NaBH_4$) has been given in Fig. 5d, here the slope value is calculated to be 0.051, hich is negligible and indicates a ero-order reaction kinetics [59]. NaOH is often used as a stabili ing agent to prevent the self-h drol sis of $NaBH_4$. Fig. S7 sho s the effect of NaOH concentration on h drogen

generation from $NaBH_4$ h drol sis, hich indicates that the addition of NaOH can greatl promote the catal tic h drol sis of $NaBH_4$. Notabl , the H_2 generation rate remains almost unchanged hen the NaOH concentration is increased from 0.4 t% to 10 t%. Therefore, e select 0.4 t% as the optimal NaOH concentration in this ork, hich can avoid asting the reagent.

The effect of temperature on h drogen generation rate is studied in the range of 298 K–318 K (Fig. 6a and Fig. S8). The results sho an increase in HGR ith the increase in reaction temperature. According to the Arrhenius plot, the calculated E_a of Ru/Co_6Ce_1@ZIF-67 and Ru/Co@ZIF-67 are 53.0 kJ mol^{-1}, hich are slightl lo er than that of Ru/Ce@ZIF-67 (54.0 kJ mol^{-1}) (Fig. 6b). The reusabilit of Ru/Co_6Ce_1@ZIF-67 in $NaBH_4$ h drol sis at 25 °C are probed using the same catal st in 5 successive c cles. As displa ed in Fig. 6c–d, H_2 ields over ve c cles are almost the same (taking appro i-matel 6.2, 7.2, 8.5, 9.8 and 10.5 min, respectivel), and the TOF values decrease each time slightl . After ve c cles, Ru/Co_6Ce_1@ZIF-67 catal st still preserves its pristine morpholog , e cept that some Ru clusters fall off from the surface (Fig. S9). As can be seen from Fig. S10, compared ith the initial catal st, the content ratio of Ru, Co^{2+}, Ce^{3+} is slightl increased, indicating the partial RuO_2, Co^{3+} and Ce^{4+} have been reduced in the process of h drol sis. Ho ever, the XPS spectra of O 1 sho that the o gen vacanc concentration is reduced from 26.3% to 17.0%. Thus, the slight decrease in catal tic activit ma be mainl attributed to Ru clusters e foliation, decreased o gen vacanc concentration and poisoning [60].

Catalytic mechanism analysis

Based on the above anal sis, the proposed mechanism for the catal tic h drol sis of $NaBH_4$ is sho n in Fig. 7. From the above XPS stud , it can be kno n that the binding energ of Ru clusters in Ru/Co_6Ce_1@ZIF-67 is negativel shifted compared to Ru/Ce@ZIF-67, suggesting electrons are transferred from Co o ides to Ru clusters. Consequentl , the electron densit of the Co o ides is greater than Ru clusters. Hence, BH_4^- takes place a reversible dissociation on active sites of Co o ides and Ru clusters, resulting in electron-de cient BH_3^- adsorbed on Co o ides sites, and H adsorbed on Ru clusters sites. The negative charge of BH_3^- is transferred to H through o gen vacancies [61]. The adsorbed H reacts ith an H from free ater to release H_2. The BH

Appendix A. Supplementary data

Supplementar data to this article can be found online at https://doi.org/10.1016/j.ijh dene.2022.08.289.

REFERENCES

[1] Zhang Y, Long X, Liu X, Chen G, Zhang N, Li M, et al. Superlattice-like Co-doped Mn o ide and NiFe h dro ide nanosheets to ard an energetic o gen evolution reaction. ACS Sustainable Chem Eng 2022;10:5683–92.

[2] Shao X, Yang Y, Liu Y, Yan P, Zhou S, Ta lor Isimjan T, et al. O gen vacanc -rich N-doped carbon encapsulated BiOCl-CNTs heterostructures as robust electrocatal st s nergisticall promote o gen reduction and Zn-air batteries. J Colloid Interface Sci 2022;607:826–35.

[3] Wang F, Zhang Y, Zhang J, Yuan W, Li Y, Mao J, et al. In situ electrochemicall formed Ag/NiOOH/Ni_3S_2 heterostructure electrocatal sts ith e ceptional performance to ard o gen evolution reaction. ACS Sustainable Chem Eng 2022;10:5976–85.

[4] Peng Q, Shao X, Hu C, Luo Z, Ta lor Isimjan T, Dou Z, et al. Co_4S_3 grafted 1 T-phase dominated WS_2 ultrathin nanosheet arra s for highl ef cient overall ater splitting in alkaline media. J Colloid Interface Sci 2022;615:577–86.

[5] He F, Han Y, Tong Y, Zhong M, Wang Q, Su B, et al. NiFe allo s@N-doped graphene-like carbon anchored on N-doped graphiti ed carbon as a highl ef cient bifunctional electrocatal st for o gen and h drogen evolution reactions. ACS Sustainable Chem Eng 2022;10:6094–105.

[6] Abdelhamid HN. A revie on h drogen generation from the h drol sis of sodium boroh dride. Int J H drogen Energ 2021;46:726–65.

[7] Ou ang L, Zhong H, Li H-W, Zhu M. A rec cling h drogen suppl s stem of $NaBH_4$ based on a facile regeneration process: a revie . INORGA 2018;6:10.

[8] Tuan DD, Huang C-W, Duan X, Lin C-H, Lin K-YA. Cobalt-based coordination pol mer-derived he agonal porous cobalt o ide nanoplate as an enhanced catal st for h drogen generation from h drol sis of boroh dride. Int J H drogen Energ 2020;45:31952–62.

[9] Nunes HX, Silva DL, Rangel CM, Pinto AMFR. Reh drogenation of sodium borates to close the $NaBH_4$-H_2 c cle: a revie . Energies 2021;14:3567.

[10] Kojima Y, Ka ai Y, Nakanishi H, Matsumoto S. Compressed h drogen generation using chemical h dride. J Po er Sources 2004;135:36–41.

[11] Boran A, Erkan S, O kar S, Eroglu I. Kinetics of h drogen generation from h drol sis of sodium boroh dride on Pt/C catal st in a o reactor. Int J Energ Res 2013;37:443–8.

[12] Cho dhur AD, Agnihotri N, De A. H drol sis of sodium boroh dride using Ru–Co-PEDOT nanocomposites as catal st. Chem Eng J 2015;264:531–7.

[13] Zhang Y, Zou J, Luo Y, Wang F. Stud on preparation and performance of Ru-Fe/GO catal st for sodium boroh dride alcohol sis to produce h drogen. Fullerenes, Nanotub Carbon Nanostruct 2020;28:786–93.

[14] Lu D, Yu G, Li Y, Chen M, Pan Y, Zhou L, et al. RuCo NPs supported on MIL-96(Al) as highl active catal sts for the h drol sis of ammonia borane. J Allo s Compd 2017;694:662–71.

[15] Wu C, Guo J, Zhang J, Zhao Y, Tian J, Isimjan TT, et al. Palladium nanoclusters decorated partiall decomposed porous ZIF-67 pol hedron ith ultrahigh catal tic activit and stabilit on h drogen generation. Rene Energ 2019;136:1064–70.

[16] Paladini M, Ar ac GM, Godinho V, Hufschmidt D, de Haro MCJ, Beltrán AM, et al. The role of cobalt h dro ide in deactivation of thin lm Co-based catal sts for sodium boroh dride h drol sis. Appl Catal B Environ 2017;210:342–51.

[17] Yao L, Li X, Peng W, Yao Q, Xia J, Lu Z-H. Co-CeO nanoparticles anchored on a nitrogen-doped carbon nanosheet: a s nergistic effect for highl ef cient h drol sis of sodium boroh dride. Inorg Chem Front 2021;8:1056–65.

[18] Liu H, Shi Q, Yang Y, Yu Y-N, Zhang Y, Zhang M, et al. CoO-Co_2P composite nanosheets as highl active catal sts for sodium boroh dride h drol sis to generate h drogen. Funct Mater Lett 2020;13.

[19] Wei L, Dong X, Ma M, Lu Y, Wang D, Zhang S, et al. Co_3O_4 hollo ber: an ef cient catal st precursor for h drol sis of sodium boroh dride to generate h drogen. Int J H drogen Energ 2018;43:1529–33.

[20] Wu C, Zhang J, Guo J, Sun L, Ming J, Dong H, et al. . . coordao

s nergisticall catal e the $NaBH_4$ h drol sis and electro-reductive H_2 evolution. ChemCatChem 2021;13:3628–35.
[33] Wang Q, Gao F, Xu B, Cai F, Zhan F, Gao F, et al. ZIF-67 derived amorphous $CoNi_2S_4$ nanocages ith nanosheet arra s on the shell for a high-performance as mmetric supercapacitor. Chem Eng J 2017;327:387–96.
[34] Gao T, Li X, Chen X, Zhou C, Yue Q, Yuan H, et al. Ultra-fast preparing carbon nanotube-supported trimetallic Ni, Ru, Fe heterostructures as robust bifunctional electrocatal sts for overall ater splitting. Chem Eng J 2021;424:130416.
[35] Yang Y, Huang Y, Zhou S, Liu Y, Shi L, Isimjan TT, et al. Delicate surface vacancies engineering of Ru doped MOF-derived Ni-NiO@C hollo microsphere superstructure to achieve outstanding h drogen o idation performance. J Energ Chem 2022;72:395–404.
[36] Cao Y, Su Y, Xu L, Yang X, Han Z, Cao R, et al. O gen vacanc -rich amorphous FeNi h dro ide nanoclusters as an ef cient electrocatal st for ater o idation. J Energ Chem 2022;71:167–73.
[37] L u F, Bai Y, Li Z, Xu W, Wang Q, Mao J, et al. Self-templated fabrication of CoO–MoO_2 nanocages for enhanced o gen evolution. Adv Funct Mater 2017;27:1702324.
[38] Lai J, Huang B, Chao Y, Chen X, Guo S. Strongl coupled nickel–cobalt nitrides/carbon h brid nanocages ith Pt-like activit for h drogen evolution catal sis. Adv Mater 2019;31:1805541.
[39] K on IS, Debela TT, K ak IH, Park YC, Seo J, Shim JY, et al. Ruthenium nanoparticles on cobalt-doped 1T′ phase MoS_2 nanosheets for overall ater splitting. Small 2020;16:2000081.
[40] Liu J, Zheng Y, Jiao Y, Wang Z, Lu Z, Vasileff A, et al. NiO as a bifunctional promoter for RuO_2 to ard superior overall ater splitting. Small 2018;14:1704073.
[41] Gao Z, Fan G, Liu M, Yang L, Li F. Dandelion-like cobalt o ide microsphere-supported RuCo bimetallic catal st for highl ef cient h drogenol sis of 5-h dro meth lfurfural. Appl Catal B Environ 2018;237:649–59.
[42] Li D, Zhang Q, Shen Z, Siddharth K, Chen L, Shao M, et al. 3D he apod-shaped Co-ZIFs-S derived co nanoparticles embedded into nitrogen and sulfur co-doped carbon decorated ith ruthenium nanoparticles as ef cient catal st for rechargeable lithium o gen batter . Nano Energ 2022;91:106644.
[43] Zhou S, Yang Y, Zhang W, Rao X, Yan P, Isimjan TT, et al. Structure-regulated Ru particles decorated P-vacanc -rich CoP as a highl active and durable catal st for $NaBH_4$ h drol sis. J Colloid Interface Sci 2021;591:221–8.
[44] Hu Y, Yu H, Qi L, Dong J, Yan P, Ta lor Isimjan T, et al. Interface engineering of needle-like P-doped MoS_2/CoP arra s as highl active and durable bifunctional electrocatal st for overall ater splitting. ChemSusChem 2021;14:1565–73.
[45] Wang C, Shang H, Li J, Wang Y, Xu H, Wang C, et al. Ultralo Ru doping induced interface engineering in MOF derived ruthenium-cobalt o ide hollo nanobo for ef cient ater o idation electrocatal sis. Chem Eng J 2021;420:129805.
[46] Li T, Zhang X, Chen Y, Zhong L, Li S, Zhang P, et al. Boosting the ater dissociation kinetics via charge redistribution of ruthenium decorated on S, N-codoped carbon. J Mater Chem 2021;9:16967–73.
[47] Guo Y, Hong X, Wang Y, Li Q, Meng J, Dai R, et al. Multicomponent hierarchical Cu-doped NiCo-ldh/CuO double arra s for ultralong-life h brid ber supercapacitor. Adv Funct Mater 2019;29.
[48] Li Q, Huang F, Li S, Zhang H, Yu X-Y. O gen vacanc engineering s nergistic ith surface h drophilicit modi cation of hollo Ru doped CoNi-ldh nanotube Arra s for boosting h drogen evolution. Small 2022;18:2104323.
[49] Li Z, Zhang Y, Feng Y, Cheng C-Q, Qiu K-W, Dong C-K, et al. Co_3O_4 nanoparticles ith ultrasmall si e and abundant o gen vacancies for boosting o gen involved reactions. Adv Funct Mater 2019;29:1903444.
[50] Zhong H, Alberto Estudillo-Wong L, Gao Y, Feng Y, Alonso-Vante N. O gen vacancies engineering b coordinating o gen-buffering CeO_2 ith CoO nanorods as ef cient bifunctional o gen electrode electrocatal st. J Energ Chem 2021;59:615–25.
[51] Yao Q, Lu Z-H, Yang Y, Chen Y, Chen X, Jiang H-L. Facile s nthesis of graphene-supported Ni-CeO nanocomposites as highl ef cient catal sts for h drol tic deh drogenation